Boundary-Layer Meteorology
https://doi.org/10.1007/s10546-022-00739-0

RESEARCH ARTICLE

Tracking the Centre of Asymmetric Vortices Using Wind Velocity Vector Data Fields

Niall Bannigan[1] · **Leigh Orf**[2] · **Eric Savory**[1]

Received: 5 October 2021 / Accepted: 1 August 2022

Abstract
Tornados are a major hazard in many regions around the world and as such it is necessary to analyze them. However, such analyses require accurately tracking them first. Currently, there are gaps in the available vortex detection methods when processing a wind-field dataset to locate a series of points that are identifiable as the tornado centreline. This study proposes a novel solution that corrects for deficiencies in previous attempts to identify vortex centres when applied to tornado wind-fields, which would have otherwise led to identifying merely the region of the vortex, several potential centres requiring post-processing, or erroneously approximating the tornado centre. Additionally, this method combines the efficiency required to process large datasets of temporal and spatial wind velocity vector distributions with the accuracy needed to reliably calculate a specific line as a tornado centre. This method is compared to five other approaches commonly used for vortex identification in order to assess: (a) how accurately they identify the centre region, (b) how they handle extraneous vortices that are not of interest, and (c) their computational efficiency in processing a wind-field dataset. With the proposed method, it would be possible to plot a tornado path from formation to dissipation and perform analyses to understand the vortex characteristics with respect to this path without requiring extensive user-intervention.

Keywords Asymmetric vortices · Programmatic analysis · Tornado centre · Tornado simulation · Vortex centre tracking

1 Introduction

Tornados are rapidly rotating columns of air spawned by cumuliform clouds such as thunderstorms that make contact with the Earth's surface. The majority of significant tornados (i.e. in the range of Enhanced Fujita scale, EF, 2 to 5) develop from supercell thunderstorms (Grams et al. 2012) and, while the most violent tornados are the least common, they cause

✉ Niall Bannigan
nbanniga@uwo.ca

[1] Mechanical and Materials Engineering, University of Western Ontario, London, ON N6A 3K7, Canada

[2] Space Science and Engineering Center, University of Wisconsin-Madison, Madison, WI 53715, USA

the most damage and fatalities (Lewellen 1993). In the U.S.A., tornados have been historically responsible for a significant number of fatalities, approximately 5000 since 1950 (NCEI 2021b), and financial losses on the order of billions of dollars. For example, the tornados of Mayfield (Kentucky) in December 2021, Nashville (Tennessee) in March 2020, and several southern states in January 2017 were responsible for 93, 25, and 24 deaths and $3.9, $1.1, and $1.2 billion in damage, respectively (NCEI 2021a). For regions where tornados are most prevalent, there has been a significant reduction in fatalities over the past several decades as a direct result of improved forecasting and better alerting of the public during severe weather events (Doswell et al. 1999). Additionally, observational and numerical studies of tornados have improved the understanding of their behaviour, allowing for longer tornado warning lead-times (Brooks and Correia 2018) and the development of better design codes for buildings to withstand the wind-loading of a tornado (Agee and Taylor 2019). Despite these advances, the available options for accurately pinpointing their paths in advance of their formation are limited, not to mention the tornado warning false alarm rate is about 75% in the United States (Lim et al. 2019).

1.1 Background of Tornado Modelling

Many attempts have been made to develop models for tornados—absent their parent storm—to identify the key characteristics of formation, translation, and structural wind-loading generation. Analytical models, often used as reference, include those of Kuo (1971) and Wen and Ang (1975). Attempts to model tornados experimentally include the Ward-type vortex simulator (Ward 1972), later modified to the Purdue simulator (Church et al. 1979), and more recently the large-scale WindEEE dome (Refan and Hangan 2016). Similarly, tornado vortex chamber (TVC) models have been developed using computer simulation techniques that make use of large-eddy simulation (LES) (e.g. Liu et al. 2018) or Reynolds-averaged Navier–Stokes (RANS) models (e.g. Natarajan 2011). Recently, cloud model simulations of supercell thunderstorms have been conducted at a high resolution to permit the formation of physically realistic tornados within the simulation (e.g. Orf 2019). This contrasts with the much simpler computational fluid dynamics, CFD, approaches where tornados are forced externally by artificially imposed boundary conditions. These physically based, simulated tornados exhibit much of the behaviour of observed storms but require massively parallel supercomputers to execute. One such simulation is the subject of the vortex identification and tracking method described herein.

The extraction of useful results from any type of simulated tornado involves comparing between analytical models, chamber models, numerical simulations, and real-world tornados to validate and critique the velocity and/or pressure-fields in the data (e.g. Natarajan 2011; Refan and Hangan 2016; Baker and Sterling 2017). It should be noted that many models are engineering-focussed (e.g. Wen 1975; Savory et al. 2001; Shehata et al. 2005; Refan et al. 2017; Liu et al. 2018) and, thus, are idealized, reduced-scale, subsets of the more realistic cloud models found in meteorological research (e.g. Orf 2019). These models neglect the parent storm in simplified, uniform conditions that are imposed at the domain boundaries. To be able to quantitatively compare their results with the work of others at a common scale, researchers must first normalize the tangential velocity, u_t, profiles of the wind-field with respect to the maximum u_t. It is common practise to then generate a plot (see Fig. 1) of these data with respect to the radial distance, r, normalized to the radius of the maximum u_t (the core), R_t (e.g. Wen and Ang 1975; Natarajan 2011; Refan and Hangan 2016; Liu et al. 2018).

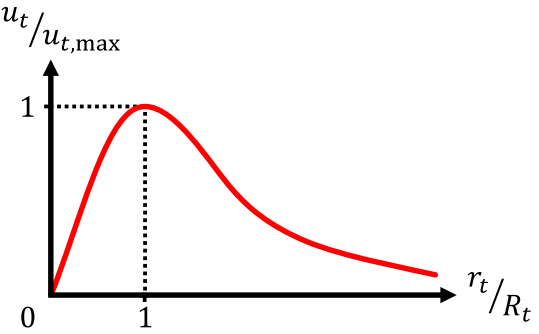

Fig. 1 Labelled example of a vortex tangential velocity profile after normalization

The concept of plotting the normalized tangential velocity against the normalized radius is derived from the Rankine vortex model (Rankine 1877). The centre of the vortex is, therefore, located where this ratio is equal to zero and crucial to providing the datum for the velocity profile for tornado analyses. However, this location is often identified without much consideration of its spatial fluctuation in time as in Tang et al. (2018). Often, it is taken at the geometric centre of the simulation chamber or domain (e.g. Church et al. 1979; Davies-Jones 2008; Altalmas and El Damatty 2013; Baker and Sterling 2017; Wang et al. 2017; Razavi and Sarkar 2018). These considerations are not an unreasonable omission for axisymmetric—the symmetry about an axis of rotation—and fixed-location models (e.g. Hamada and El Damatty 2011; Pecin et al. 2011; Altalmas and El Damatty 2014; Liu et al. 2018) or those where the tornado track is pre-defined along a set path (e.g. Beck and Dotzek 2010; Natarajan 2011; Pecin et al. 2011) since the position is known by definition. This is especially true for studies that are focussed on the accuracy of their analytical model characteristics rather than its direct similarities with atmospheric phenomena in nature (e.g. Kuo 1971; Wen 1975; Lewellen 1993; Savory et al. 2001; Davies-Jones 2008; Baker and Sterling 2017). The asymmetry and wandering of a tornado may also be considered negligible in laboratory settings at very high swirl ratios because the resulting vortex is rotating fast enough to be stable and well-defined (Refan 2014). Thus, the consideration of vortex centre motion does not have a significant effect on the results. In Wan and Chang (1972), a physical flow-field demonstrating asymmetry is simplified using a low-pass filtering process with a time constant of eight seconds to generate a temporally and spatially averaged dataset. In each of these instances, however, the described simplifications may become problematic if the instantaneous flow-field is required such as when determining the peak wind-loading present on a building.

Therefore, the present paper attempts to introduce a more robust and reliable method of tornado centre identification for the cases of non-axisymmetric and non-stationary tornados, both real-world and simulated. This does not mean, however, that the method will not also function for the more simplistic axisymmetric and stationary cases. The necessity of developing such a method can be seen in cases such as Fig. 2, where the centre of the tornado cannot clearly be identified with simplistic methods such as taking the core radius to outline the centre (Wood and Brown 1992; Refan et al. 2017) without additional processing or user-intervention. The data in Fig. 2 are a snapshot of the near-surface vector-field of the simulated tornado, analyzed herein, and demonstrate that the higher-resolution data available in more advanced simulations allow for higher precision in the tracking of tornado centres.

In this paper, the technique described is for identifying the centre of rotation as a series of point locations both spatially and temporally within a tornado. This will aid future work in

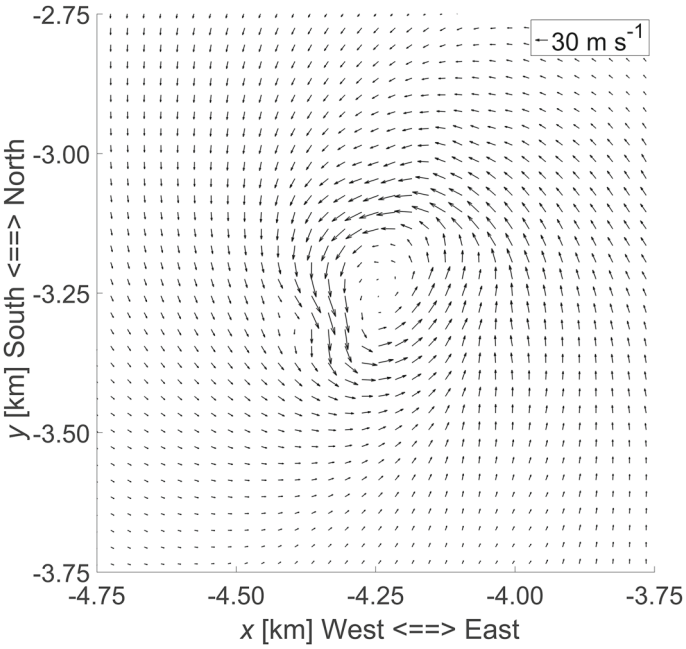

Fig. 2 Near-surface storm-relative horizontal wind-field vectors at $t = 5579$ s in the simulated tornado analyzed in the present work, indicating a snapshot in time where the tornado vortex was highly asymmetric

understanding tornado translation and the damage potential relative to their centre. Additionally, a thorough description is provided of other methods to track vortices with comparisons to the proposed one that demonstrates, for these well-resolved and highly accurate tornado simulations, the improved robustness, consistency, and precision.

1.2 Vortex Centre Identification Methods

More in-depth methods than those mentioned in the previous section for finding the centre of a tornado programmatically have been reported. For example, the use of the local maximum of the vertical component of the vorticity magnitude, ω_z, (see Fig. 3). This is found in Strawn et al. (1999) and considers the velocity derivatives on a hexahedral cell domain as part of a selection scheme (successfully used in Refan and Hangan 2016). Additionally, Potvin (2013) uses ω_z to identify regions containing potential vortices and then separates out the flow from

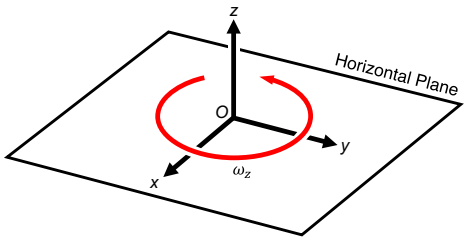

Fig. 3 Coordinate system schematic showing the vertical vorticity component of a point of interest, O, on the horizontal plane

possible vortices. Potvin (2013) does this using a modified Rankine vortex model and a cost function that, when minimized, indicates a strong relation between the wind-field and the model data. Another example is the Aboelkassem et al. (2005) application of a definition (specifically to tornado flows) that states that the vortex centre should be where the tangential velocity, pressure gradient, and vorticity gradient are all zero.

However, tornado-specific analysis has rarely involved more detailed methods of vortex core tracking such as those found in Levy et al. (1990), Jeong and Hussain (1995), Sujudi and Haimes (1995), Jiang et al. (2002), and Wong and Yip (2009). In order to rigorously track a vortex spatially and temporally it becomes necessary to use such methods and so they are employed here for comparison with the method proposed in the present paper. Table 1 summarizes the following discussion of the methods described above.

Levy et al. (1990) used the normalized helicity, H_n, of the wind-field to identify vortex structures. This scalar quantity is calculated for any given region of interest with:

$$H_n = \frac{\mathbf{u} \cdot \boldsymbol{\omega}}{|\mathbf{u}||\boldsymbol{\omega}|}, \tag{1}$$

where $\boldsymbol{\omega}$ is the vorticity given by:

$$\boldsymbol{\omega} = \nabla \times \mathbf{u} = \left(\frac{\partial u_z}{\partial y} - \frac{\partial u_y}{\partial z}\right)\widehat{\mathbf{i}} + \left(\frac{\partial u_x}{\partial z} - \frac{\partial u_z}{\partial x}\right)\widehat{\mathbf{j}} + \left(\frac{\partial u_y}{\partial x} - \frac{\partial u_x}{\partial y}\right)\widehat{\mathbf{k}}. \tag{2}$$

Additionally, $\mathbf{u} = u_x\widehat{\mathbf{i}} + u_y\widehat{\mathbf{j}} + u_z\widehat{\mathbf{k}}$ is the wind-field velocity vector where u_x, u_y, and u_z are the wind speeds in the x-, y-, and z-directions, respectively. Equation 1 represents the cosine of the angle between $\mathbf{u}$ and $\boldsymbol{\omega}$ such that when it is small the vectors are assumed by Levy et al. (1990) to be inside the vortex core. Therefore, H_n should be equal to + 1 or -1 at the centre point. This has the potential to function well for cases of multiple vortices as it can select all points that have such a H_n value. However, in Levy et al. (1990), it is noted that the angle between $\mathbf{u}$ and $\boldsymbol{\omega}$ is not necessarily small.

Jeong and Hussain (1995) introduced the λ_2 method for two- or three-dimensional velocity-fields, where λ_2 is the second eigenvalue of their derived symmetric tensor, $\mathbf{S}^2 + \boldsymbol{\Omega}^2$, for vortex identification. This method is based on the assumption that a vortex centre can be identified using local pressure minimum. Jeong and Hussain (1995) went further by only using this definition as a starting point for the cases where a pressure minimum may appear without a vortex or a vortex may appear without a pressure minimum. They defined the strain-rate tensor, $\mathbf{S}$, as

$$\mathbf{S} = \frac{1}{2}\left(\nabla\mathbf{u} + (\nabla\mathbf{u})^{\mathrm{T}}\right), \tag{2.1}$$

and the spin tensor, $\boldsymbol{\Omega}$, as

$$\boldsymbol{\Omega} = \frac{1}{2}\left(\nabla\mathbf{u} - (\nabla\mathbf{u})^{\mathrm{T}}\right), \tag{2.2}$$

which are the symmetric and antisymmetric elements, respectively, of the velocity gradient tensor (given for the two-dimensional case):

$$\nabla\mathbf{u} = \begin{pmatrix} \frac{\partial u_x}{\partial x} & \frac{\partial u_y}{\partial x} \\ \frac{\partial u_x}{\partial y} & \frac{\partial u_y}{\partial y} \end{pmatrix}. \tag{2.3}$$

Table 1 Summary of main characteristics of previous vortex identification methods

Analysis method	Benefits	Drawbacks
Levy et al. (1990)	Simple analytical relation Able to handle multiple vortices	Requires 3D data analysis Criterion for detection is not necessarily true for all vortices Identifies a line of vorticity
Jeong and Hussain (1995)	Simple analytical relation Able to handle multiple vortices	Cannot distinguish clustered vortices Identifies a core region only
Sujudi and Haimes (1995)	Uses mathematical relation Capable of identifying vortex as a point	Requires 3D data analysis
Jiang et al. (2002)	Simple criterion, easily implemented No specific data grid type Capable of identifying vortex as a point Able to handle multiple vortices	Cannot distinguish clustered vortices without expensive iteration process
Wong and Yip (2009)	Able to handle skewed data grids Identifies vortex as a point	Requires extensive user input to function at all

Then, a vortex region is defined where $\lambda_2 < 0$ given that λ_2 is the second largest eigenvalue of the symmetric tensor, which can be expressed according to Chen et al. (2015) as

$$\lambda_2 = \left(\frac{\partial u_x}{\partial y}\frac{\partial u_y}{\partial x} - \frac{\partial u_x}{\partial x}\frac{\partial u_y}{\partial y}\right) + \frac{1}{2}\left(\frac{\partial u_x}{\partial x} + \frac{\partial u_y}{\partial y}\right)^2 + \frac{1}{2}\left|\frac{\partial u_x}{\partial x} + \frac{\partial u_y}{\partial y}\right|\sqrt{\left(\frac{\partial u_x}{\partial x} - \frac{\partial u_y}{\partial y}\right)^2 + \left(\frac{\partial u_x}{\partial y} + \frac{\partial u_y}{\partial x}\right)^2}. \tag{2.4}$$

Jeong and Hussain (1995) note that this definition of a vortex is versatile and can work for centre identification reliably in several flow-field applications. According to Jiang et al. (2005), this method is not able to easily identify individual vortices. However, this may be useful in cases where there are many equally powerful vortices clustered together that need to be analyzed as a group to identify the dominant vortex. This method does not identify a point as the vortex centre but, rather, the general region of the vortex core.

Sujudi and Haimes (1995) developed an algorithm for checking the divided, three-dimensional regions, or mesh cells, of any shape in a simulation dataset for critical points. The critical points are defined at locations where the slope of the fluid flow streamlines is not definite and the storm-relative velocity is equal to zero. The rate of change of the deformation tensor is computed from the coefficients of a trilinear interpolation function for the fluid velocity in each direction:

$$\mathbf{A} = \begin{bmatrix} \frac{\partial u_x}{\partial x} & \frac{\partial u_y}{\partial x} & \frac{\partial u_z}{\partial x} \\ \frac{\partial u_x}{\partial y} & \frac{\partial u_y}{\partial y} & \frac{\partial u_z}{\partial y} \\ \frac{\partial u_x}{\partial z} & \frac{\partial u_y}{\partial z} & \frac{\partial u_z}{\partial z} \end{bmatrix}. \tag{2.5}$$

Then, the eigenvalues, λ_i, of the matrix $\mathbf{A}$ are computed and checked such that the critical point search should continue only if there is a real eigenvalue and a pair of complex-conjugate eigenvalues. This is reminiscent of the approach developed by Jeong and Hussain (1995), described above. Then, for $\mathbf{u}$ at each node, the eigenvector of the real eigenvalue, $\mathbf{v}_i$, is subtracted to yield a reduced velocity as

$$\mathbf{w} = \mathbf{u} - \frac{\mathbf{u} \bullet \mathbf{v}_i}{||\mathbf{v}_i||^2}\mathbf{v}_i, \tag{2.6}$$

where $||\mathbf{v}_i||$ is the norm of the eigenvector and each component, w_i, is the equation of a plane. If w_i of just two components is set to 0, then they must intersect, which, for two planes, is a line. Should the line formed by these two planes intersect with two different faces on the cell then the cell is said to contain part of a vortex. The authors also suggest a more efficient approach, whereby the programme finds exactly two points on each cell for two different faces where $\mathbf{w} = 0$ and uses these to define the line of local swirling flow without compromising accuracy. Orf et al. (2007) successfully implemented this method and showed that it can identify specific vortex point locations, unlike Jeong and Hussain's (1995) method.

Jiang et al. (2002) developed a combinatorial topology method, utilizing the principle of Sperner's lemma, which is an algorithm for detecting regions of core vortex rotation (Rosen 2000). The points in an area of interest are labelled according to the range of directions they face, meaning that vectors can be categorized within the wind-field to be compared with other points in a given area (see Fig. 4a).

Notably, this method can apply to flow-field data of both structured and unstructured grids. The points immediately around each point of interest are evaluated to determine if all of the categories are present in such a way that the area contained between the identified vertices

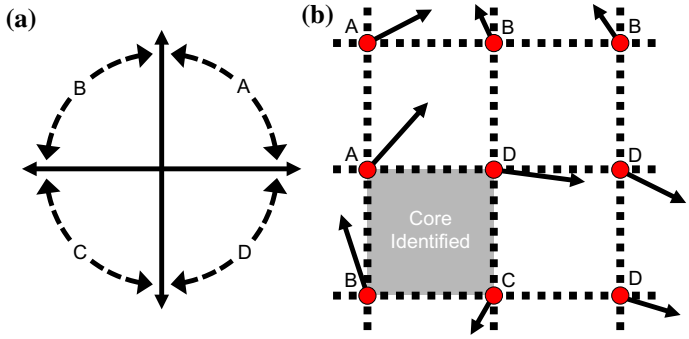

Fig. 4 Schematic diagram representing the direction spanning vortex identification method in Jiang et al. (2002). **a** Defining four vector label ranges (A–D) based on orientation and **b** example vector-field with an identified core region using a structured Cartesian grid system

is a vortex (see Fig. 4b). This method, alone, does not explicitly identify a single point as the centre, but, by interpolating the vector-field, can do so through iteration until the area enclosed by the vertices is sufficiently small that it may be approximated as a point. This method is also capable of identifying multiple vortices while only generating some false positives in complex flow-fields, as noted by the authors.

Wong and Yip (2009) present a method of locating the centre of a rotation in circulating and spiralling vector flow-fields by creating a logarithmic spiral to align with a given flow-field that could identify the pattern of the flow using

$$r = ae^{\theta \cot \alpha},$$

where r is the radius of a point on the spiral from its centre, a is the rate of growth of the spiral and determines the direction of rotation, θ is the angle with respect to the x-axis in a polar coordinate system, and α is the angle of the radial line from the centre to the tangent of the spiral at position (r, θ). Since Wong and Yip (2009) also worked with cases of centre location at oblique viewing angles to the wind-field plane, they redefined α as ψ using an additional parameter, ρ, to hold the viewing angle such that only when the viewing angle is normal to the plane are the two parameters equivalent. Following this, the vectors are all rotated by $\pi - \psi$ to force them to point to the centre of the spiral. Thus, the centre of the rotation is identified as the point with the most intersections, n_c, of the area spanning $\sigma + \sigma^+$ from each of the rotated vector tips. If the viewing angle is normal to the plane, $\sigma = 0$. The sector expansion angle,σ^+, is defined by the user to increase the chance of the true centre being found in distorted or partial datasets. For the cases where the viewing angle is oblique, this location is identified by the greatest overlap of the region that extends at an angle $\psi_{\max} - \psi_{\min}$ from the tip of the rotated vectors. The authors acknowledged that this method requires α and ρ to be known a priori and that the general region of the centre needs to be identified first in order to avoid errors (e.g. in cases of multiple vortices in proximity). Thus, the algorithm's utility for the automation of the centre identification and tracking process is greatly reduced.

Although each of the aforementioned methods in this section has relevant applications in tornado modelling and research, they are unable to precisely identify the centre of a tornado while meeting the following criteria: (1) output a single point on a data-grid plane as the centre location, (2) operate in a computationally efficient manner, and (3) require minimal user-input or a priori information in order to function. To relate key characteristics of tornados to the

radius from the vortex centre and precisely track translation during their lifespans—even when there is not just a single, well-defined, axisymmetric vortex—requires the introduction of a novel method, which is the objective of the present work.

1.3 Tornado Centre Identification

In this paper, the data used were captured from a large-scale supercell simulation performed on the National Centre for Supercomputing Applications (NCSA) Blue Waters supercomputer using a modified version of the Bryan Cloud Model, version 1 (CM1) model (Bryan and Fritsch 2002; Bryan 2008). CM1 is a three-dimensional, nonhydrostatic, fully compressible cloud model designed for idealized studies of atmospheric phenomena such as thunderstorms. CM1 contains prognostic variables for wind, potential temperature, pressure, turbulence kinetic energy, cloud water, cloud ice, rain, snow, and hail/graupel. The model has been tuned to run efficiently on modern massively parallel supercomputer architectures and has produced some of the highest resolution thunderstorm simulations conducted to date (e.g. Orf 2019). The tornado used in the development of the present method was produced in such a simulation. This generated a large amount of data points and timesteps necessitating the use of a centre-tracking algorithm for any type of analysis, as outlined in the previous section.

From 25 to 27 April 2011, central and south-eastern U.S.A. experienced one of the largest tornado outbreaks ever recorded, with 348 tornado-related deaths and over $10 billion of damage (NCEI 2021a). The simulation analyzed in this work was executed within 27 April 2011 mid-afternoon environmental conditions upwind of the day's outbreak where a record 216 tornados were observed. The tornado from the simulation that is utilized in the present paper appears to be representative of one of the 30 tornados rated EF3 and EF4 that occurred during the real-life event (Curtis and Mills 2012; Karstens et al. 2013), with peak tangential wind velocities relative to the domain of approximately 75 m s^{-1} and a core diameter of 500 m.

Thirteen-hundred seconds of three-dimensional velocity data at 30 m grid resolution and single-second timesteps, spanning much of the tornado's life, were analyzed with the vortex tracking code described in this paper. Finley et al. (2018) presented preliminary results from a simulation in this same environment where a violent long-path tornado formed. As is the case with all of the CM1 simulations described, the tornado formed naturally within the three-dimensional environment, unconstrained by artificial symmetries or external forcing as in TVC simulations. The tornado was freely able to move and tilt within the domain of 160 km in each horizontal dimension and 20 km vertically. However, a constant horizontal velocity vector ($\mathbf{u_{move}} = \langle 15.2,\ 10.5 \rangle$ m s^{-1}) was subtracted from the velocity data to account for this free motion. Thus, a smaller, sample subdomain of approximately 3.3-by-5.7 km horizontally and 330 m vertically was extracted from within the simulation domain, effectively capturing the tornado by moving with it through the storm. This sample domain is the only volume of the simulation used in the analysis performed in this study.

It became apparent that the other methods of vortex centre identification, used previously in tornado model work and discussed above, are insufficient if attempting to analyze these data using a coordinate system defined with the tornado centre as the origin. This study presents a novel programmatic method of vortex identification that is relevant to the field of tornado vortex simulation and greatly improves the precision of both centre tracking and the subsequent data analyses taken with respect to that centre.

2 Methodology Details

When analyzing wind-field data from a tornado, or any given vortex, it is helpful to know the relative position of a point of interest with respect to the centre of the rotation and to identify that centre in a consistent way to track its motion in space and time. Details of the unpacking of the tornado simulation wind-field data and the assumptions and method involved in tracking the centre of the vortex are given in the following section and concisely summarised by the series of equations found in Appendix 1.

2.1 Data Processing

The tornado wind-field data from the numerical simulation, based on an isotropic 30 m mesh, are organized in Cartesian coordinates and, thus, to best analyze them with respect to the centre of the vortex, it is necessary to convert them into cylindrical coordinates with their origin at the centre and base of the tornado. Each file contains an array for each of the velocity components in the x-, y-, and z-directions as u_x, u_y, and u_z, respectively. These velocities need to be converted to tangential, radial, and vertical velocity components u_t, u_r, and u_z, respectively, with respect to the vortex centre (O), as shown in Fig. 5.

The cylindrical coordinate system components are defined as r for the radius from O, θ for the angle with respect to the x-axis of the Cartesian coordinate, and z for the vertical axis (the same as in the Cartesian coordinates). This tornado is fully three dimensional as opposed to axisymmetric; hence, before locating the centre of the vortex, it is necessary to describe how that centre should be defined. In this study, the tornado centre is defined in the region where the gradient of **u** is a local minimum and is surrounded by a significant number of vectors displaying large curl in the horizontal plane and, ultimately, where u_x and $u_y = 0$ m s^{-1} (Rankine 1877; Wong and Yip 2009). The analysis begins, therefore, by considering only one horizontal slice of data at a time so that the analyses are in two dimensions. The results

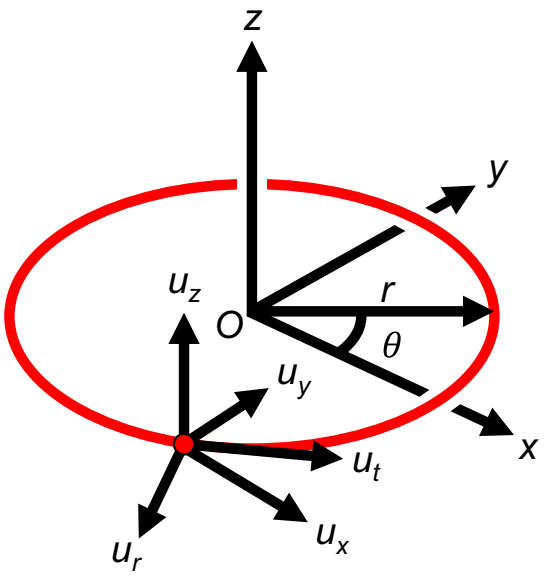

Fig. 5 Cylindrical coordinate system conversion schematic

of each individual analysis do not affect any subsequent analyses and therefore can be solved for either sequentially or concurrently. The velocity vector curl is simply the vorticity, $\boldsymbol{\omega}$, and is determined using Eq. 2 for a two-dimensional plane. The velocity vectors of interest are those located near where $\boldsymbol{\omega}$ is a local maximum. There may be cases where multiple equally well-defined tornados appear in these supercell simulations, as well as in nature (Orf et al. 2016). However, in the present work, there is clearly a single dominant tornado vortex that encounters partial and minor vortices in the simulation. A schematic example of the wind-field is shown in Fig. 6a before any coordinate conversion has been performed and with vector arrows representing $\mathbf{u}$. The number of local maxima of $\nabla \times \mathbf{u}$ identified is determined by:

$$n = \frac{\min\lfloor n_x, n_y \rceil}{c}, \tag{3}$$

where n is the scaling-factor rounded to the nearest integer based on the size of the dataset, n_x is the number of points in x, n_y is the number of points in y, and c is the scaling parameter that is determined through a trial-and-error approach. The $\lfloor$ and $\rceil$ brackets are used together here to indicate that the fractional components of values are rounded, down if less than 0.5 or up if 0.5 or greater, to the nearest integer, respectively. Equation 3 is used to ensure that, for a given dataset size and resolution, the number of points used for vortex detection is not so few that the search results are inconclusive and not so many that the points identified begin to include those that are not part of a well-defined vortex. For this study, n_x is 190, n_y is 111,

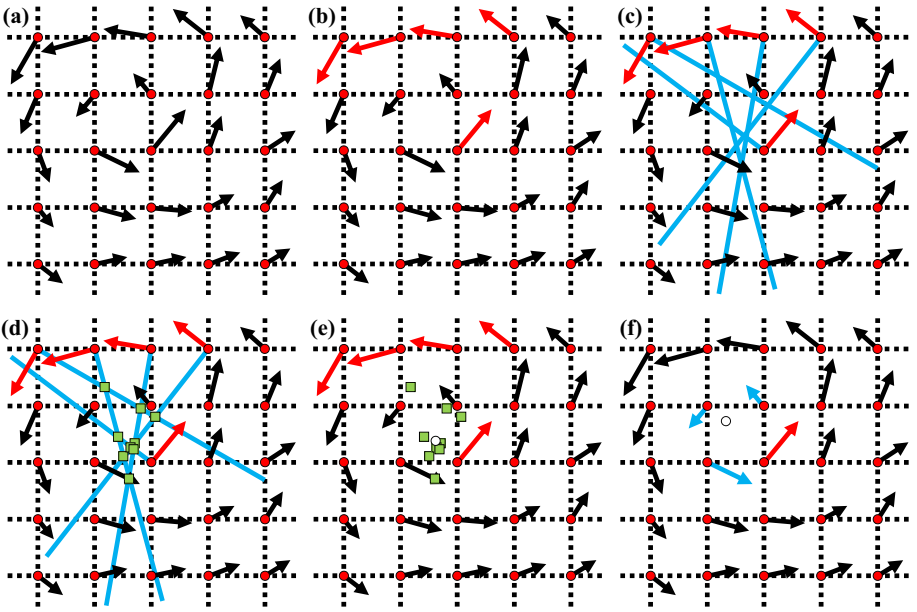

Fig. 6 Finding the centre of an asymmetric vortex system using artificial data for illustrative purposes as an example where $n_{scale} = 5$. **a** Schematic example of tornado dataset with vectors (shown as black arrows) on an isotropic grid (shown as dashed lines), **b** 5 vectors (shown in red) selected based on n_{scale}, **c** lines perpendicular to the selected vectors' orientation drawn (shown in blue), **d** identified intersections of each line drawn (shown as green squares), **e** location of average intersection identified (shown as white circle), and **f** nearest vector identified (shown in red) and nearest vectors from identified vector that complete a loop (shown in blue) then used to interpolate for the location of zero-velocity (shown as white circle)

and c is set at a value of 6 (see Appendix 2 for comparison of the impact of c values on the results). Therefore, $n = 19$ and the largest n values of $\nabla \times \mathbf{u}$ are identified (schematically shown in Fig. 6b using $n = 5$, as an example). Following this selection, the spatial averages (indicated by $\langle$ and $\rangle$ brackets) of the x and y positions of the maximum curl locations, x_c and y_c, and their standard deviations, σ_x and σ_y, are computed. Note that σ_x and σ_y are always rounded up since x_c and y_c are indexed positions, not interpolated. By rounding up, this method provides a more conservative approach to the number of points eliminated from the search within each standard deviation. Using a desired number of standard deviations, s, the next step is to eliminate all points from the centre search that fall outside of the area of the ellipse centred on $[\langle x_c \rangle, \langle y_c \rangle]$ of lengths $2s^{1/2}\sigma_x$ and $2s^{1/2}\sigma_y$ using:

$$\frac{\left(x_{c,i} - \langle x_c \rangle\right)^2}{\left(\sigma_x\right)^2} + \frac{\left(y_{c,i} - \langle y_c \rangle\right)^2}{\left(\sigma_y\right)^2} \leq s. \tag{4}$$

It should be noted that, if multiple vortices are present in a given dataset, an additional step should be inserted here to weight the filtering of selected points by location relative to other identified maximum curl positions. The analysis would then proceed for each identified region regardless of how many vortices are present. The remaining number of points, $N = 1, 2, \ldots$, is refined further using a technique developed from the methodology used by Wong and Yip (2009) to find the centre of rotating fields at any given angle of observation to the plane of rotation. Their technique is not applied directly here because, as mentioned in Sect. 1, it requires knowledge of the location of the vortex region within the domain before applying the analysis technique and it is designed for axisymmetric-dominant systems. In the present study, the data are often highly asymmetric during the tornado's lifetime. This includes the presence of a secondary, smaller vortex close to the main vortex that could skew the results considerably if Wong and Yip's (2009) method was to be applied directly (see Sect. 3). Thus, the principle of using the overlapping of all the regions of confidence extending from the rotated velocity vector tips to identify the centre has been adapted so that lines perpendicular to the velocity vector directions are drawn at each of the n locations of x_c and y_c, minus those that did not satisfy Eq. 4. This is achieved by determining the equation of a line perpendicular to the identified velocity vectors (see Fig. 6c). The intersections of these lines are identified by setting the x and y in the equation of a given line equal to the x and y of another (Fig. 6d), which results in

$$x_t = \frac{b_j - b_i}{m_i - m_j},$$
$$y_t = \frac{m_j b_i - m_i b_j}{m_j - m_i},$$

where x_t and y_t are the x and y positions of the line intersections, respectively, b is the y-intercept of the lines with the domain ordinate, m is the slope of the lines, and i refers to the first line selected and varies from 1 to $N - 1$ in an incremental loop to be compared with line j, which varies from $i + 1$ to N in an incremental loop contained within i to avoid comparing the same intersection with itself or double counting intersections.

A similar averaging technique to that applied to the maximum vorticity locations is also used here for the intersections. The standard deviation and point elimination techniques above are applied, with the addition that any intersection outside of the domain is ignored before averaging (see Fig. 6e). Then, the position of this final averaged point of intersections is checked for an indication that either it does not fall within the selection region or the location is so close to the domain edge that the programme will attempt to search outside of it in the

subsequent centre searching process. In the case of a null error, the location found will be replaced with the location of maximum z-direction vorticity in the wind-field or the minimum pressure that are both able to approximately, but not exactly, identify a centre.

The average, although very useful in narrowing the area of search, is not used directly to find the centre position as it is less accurate for the times in the tornado data where the shape of the vortex is highly asymmetric. Instead, the point in the data nearest to this point is selected (see Fig. 6f) and a c-by-c grid is created with this nearest point at the centre and the points immediately surrounding it comprising the rest of the grid. This is done under the assumption that the tornado centre will be located at the position of zero horizontal, storm-relative velocity that will likely fall somewhere in between the discrete data points. The most helpful location to begin with is at the point within this search area having the minimum velocity. Thus, a c-by-c grid is chosen as the limit of this search to keep the search within the identified vortex core and not detecting other vortices that also have a local velocity minimum, even if it is lower than that within the main vortex. In finding multiple vortices, this technique can be used on each individual vortex to find their centres rather than identifying their general region. This smaller grid is then searched to find the minimum velocity. If the previously identified point is not the minimum, then whichever point is the actual minimum velocity is defined as the centre of a three-by-three grid of the velocities of the points immediately surrounding it.

Of the remaining nine points, there are three vortex region cases checked: rotation within one of the four quadrants of the grid; rotation within the left, right, top, or bottom of the grid; or rotation about the entire grid situated about the point in the centre (see Fig. 7).

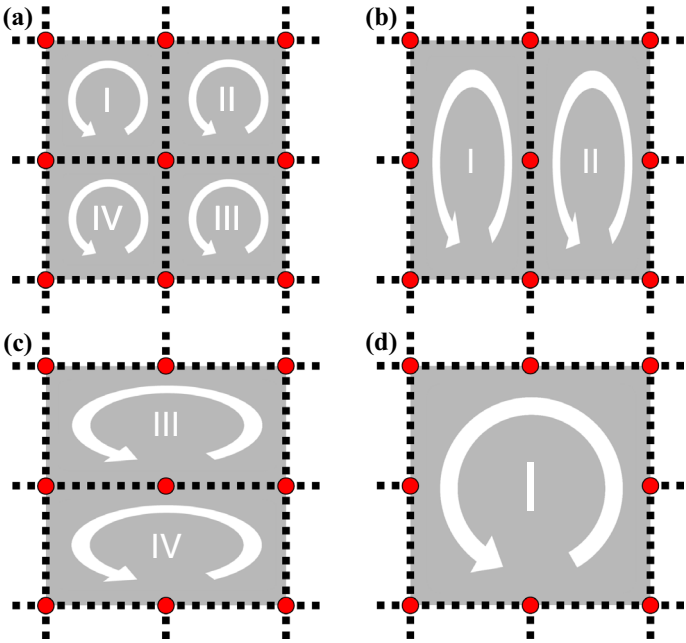

Fig. 7 Schematic view of vortex region case checking where the red circles indicate the data points. Complete rotation loop in **a** one of the four quadrants, **b** left or right halves, **c** top or bottom halves, and **d** the entire area

A complete loop is identified based on the sum of the vector signs comprising the loop adding to zero for both x- and y-directions. This is similar to the technique described in Jiang et al. (2002), although here it is able to be expanded to incorporate any desired number of points into the loop for different vortex shapes. The number of successfully identified possible loops is stored and the sum of the tangential velocity magnitudes of each vector around each path is calculated so that, for two similar paths, the one having the smallest cumulative velocity around its loop is considered to contain the centre of the vortex.

This method can be implemented iteratively, if the smaller grid size is still large, to narrow down a vortex region for larger tornados or for higher spatial resolution wind-field data where the search array may include more than c^2 vectors. If no successful path is identified, the search is repeated and skips the previously identified minimum velocity vector up to a total of c times. If this still fails to identify a path, then the point that would be substituted for the final averaged intersections in the case of error, as described above, is defaulted to as the designated tornado centre.

The four corners of the loop found above are bilinearly interpolated for the position where $u_x = 0$ and $u_y = 0$, unless no path is found in which case this interpolation step (see Fig. 10) is omitted.

Therefore, the searching portion of the algorithm is concluded, as shown in Fig. 6f, and it would be trivial to now analyze any given tornado with its centre as the origin of a cylindrical coordinate domain and make use of vortex-relative radial, tangential, and vertical velocities.

3 Results and Discussion

The results of the methods described above are detailed in the following section, including a discussion of the impact of the findings in contrast to the methods used by others described in Sect. 1.2.

3.1 Results

The programmatic methods described above were applied to the simulated tornado-producing supercell dataset as mentioned in Sect. 1. The fully tracked tornado centre may be found in Fig. 8 for both the simulation-domain-relative tracking and the ground-relative tracking. The ground-relative tracking was created by multiplying the removed velocity vector, $\mathbf{u_{move}}$, by time since the start of the dataset ($t = 5000$ s), t_s, and adding this distance to the given point associated with each timestep, respectively.

For the purpose of testing that this method functions as intended, each timestep involved an independent search of the velocity-field. To minimize computation time, it would be prudent to restrict the algorithm's search region, after the first timestep is analyzed successfully, to a distance that the tornado could not reasonably translate between timesteps.

It was apparent that the path of the vortex could be spatially and temporally defined with a high degree of accuracy, including near to the ground, which is useful in understanding the potential wind-loading on infrastructure and buildings with respect to the vortex centre. From the entirety of the 3.3-by-5.7 km^2 horizontal, 330-m-high sample domain (11 horizontal slices at 30 m spacing), the algorithm failed to interpolate for, or correctly identify, a centre position 1 time out of 1300 CM1 model timesteps when analyzed independently of each other, equating to a 0.08% error rate using $c = 6$. The timesteps where the algorithm needed to reattempt (see Sect. 2.1) identifying the centre occurred during peak u_t in the vortex,

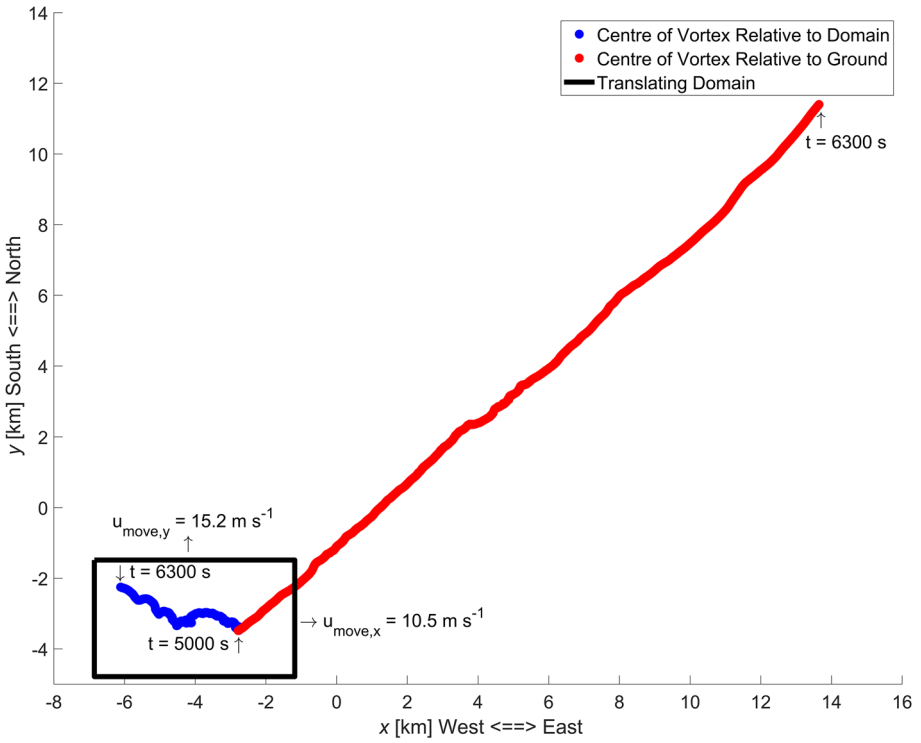

Fig. 8 Plan view of the tornado following the centre at $z = 15$ m above ground level (a.g.l.) throughout the entire life cycle of the vortex relative to the dataset domain boundaries and relative to the ground

Table 2 Comparison of the time taken to analyze a given horizontal plane of the tornado by previously developed vortex tracking methods with the proposed method

Analysis method	Analysis runtime per horizontal plane (ms)	Analysis runtime per horizontal plane (Normalized by the proposed method runtime)
Levy et al. (1990)	8.60	7.61
Jeong and Hussain (1995)	0.52	0.46
Sujudi and Haimes (1995)	8394.48	7428.74
Jiang et al. (2002)	10,786.20	9545.31
Wong and Yip (2009)	202.55	179.25
Proposed Method	1.13	1.00

approximately at the midpoint of the lifespan of the tornado, which is also when it began to combine with a weaker vortex.

3.2 Comparisons of Methods

Using the full-size of the dataset domain for several arbitrarily chosen but representative timesteps and heights a.g.l., Table 2 shows the time required to execute the searching algorithms for each of the methods detailed in Sect. 1.2 compared to the method proposed in this paper.

The fastest method is that of Jeong and Hussain (1995), with an average solution time of just 0.52 ms, followed by the proposed method in this paper and the Levy et al. (1990) method. Much slower are the methods proposed by Wong and Yip (2009), using the overlap of the spans projecting from each vector tip, by Sujudi and Haimes (1995), using the reduced velocity, and by Jiang et al. (2002), using the vector directions. The result of implementing each of these methods as intended (without modification) can be seen in Fig. 9 on a horizontal view of data, sampled from the simulation described previously.

Using the Levy et al. (1990) method, the main tornado vortex appeared to be better described by where $H_n \approx 0$ (not shown in Fig. 9) for these data. The regions where $|H_n| \approx 1$ were assumed to be those where the angle between $\mathbf{u}$ and $\boldsymbol{\omega}$ was less than or equal to 15 °. In Fig. 9, these regions seem to outline a vortex presence but do not provide a definite location of a tornado centre. Even though, as described in Levy et al. (1990), the largest ω_z was consistently within the vortex region indicating that $\boldsymbol{\omega}$ is vertical, u_z was often minuscule relative to the horizontal components of $\mathbf{u}$ such that the two vectors were not close to parallel. The sense of u_z was also not often uniform across the vortex such that the sign of H_n could not be relied upon to identify the vortex rotation direction. Additionally, to accommodate the use of the gradient operator, it was necessary to run the programme for all heights in the vortex at the single timestep because, otherwise, there would be no meaningful output. However, this only contributed to a mild increase in computational time.

Jeong and Hussain's (1995) method very effectively identifies the main vortex and (when present) a smaller, but still substantial, vortex (Fig. 9). However, it is clear that further analysis would be required to identify the centre of the tornado since its position is not given simply by $\lambda_2 < 0$ in this case.

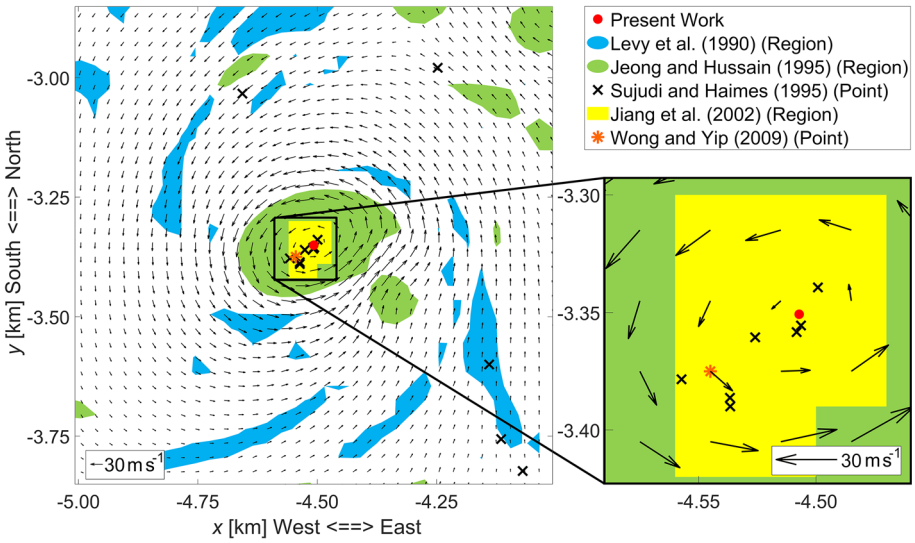

Fig. 9 Comparison of the accuracy of various methods in tracking the vortex core centre on a representative wind-field data sample at $t = 5687$ s and z = 165 m a.g.l

The method in Sujudi and Haimes (1995) is conceptually similar to the Jeong and Hussain (1995) method. However, in Sujudi and Haimes (1995), the grid of data is divided into tetrahedrons meaning six cells between every cube of eight nodes (for Cartesian coordinates) and, consequently, that two-dimensional analysis is not possible. To accommodate this, the horizontal layers above and below the layer of interest needed to be analyzed. This leads to a dramatic increase in the computation time as each cell must be created, divided, and analyzed. The advantage of this method is that it does very accurately pinpoint the location of vortices but, without filtering, does not leave one definite point (Fig. 9).

The Jiang et al. (2002) method, although the slowest of all the demonstrated methods, is able to capture the main vortex (Fig. 9). The region is a regular geometric shape because the area defined is just the region shown to capture each of the direction ranges, so it is only a binary indicator. Only the nearest neighbours to each given point of interest are analyzed, and in this comparison, the search strategy in their methodology is not implemented where the data are iterated further to group smaller vortices together into larger ones. Additionally, in this comparison, each vortex identified is not interpolated and re-analyzed to identify a centre location more precisely. To improve the precision of the vortex centre location following this method would have required much more computational time to solve and so, for the purposes of this comparison, these extra steps are omitted.

The Wong and Yip (2009) method is successful in identifying a point that is within the vortex where n_c is a maximum but this point is not the actual tornado centre (Fig. 9). The values of $\alpha = \frac{\pi}{2}$ and $\sigma^+ = \frac{\pi}{4}$ are used, as given by Wong and Yip (2009) for tornado-like vortices. For the calculation of n_c, only those points that are up to 20 points away are considered, which was determined by Wong and Yip (2009), through trial-and-error, to yield valid results. Using $\alpha = \frac{\pi}{2}$ means that the spiral is a circle, which does fit with the vector directions around the main vortex for the most part. To be able to use this method properly, the region of the main vortex would have to be identified a priori and only those vectors within this region would be a part of the span overlap analysis. Instead, the entire

domain was used for the search and so the spiral component of the method was not useful as this would defeat the purpose of an automatic searching algorithm. Although this method provides a desirable output of just a single point, for a complex and dynamic tornado system, whose centre moves within the domain, it would be useful to combine this methodology with another. For example, identifying an area of maximum vertical vorticity, such as in Potvin (2013), would narrow down the interrogation region without user-intervention.

Through the method proposed in this paper, a centre point was clearly identified (Fig. 9). This is computed using $c = 6$ and the analysis ran without error and appears to be in the correct location qualitatively as well as being the point matching the criteria for a tornado centre laid out in Sect. 2.1. Although this only captures the main vortex and not minor ones, it could (with some effort) be expanded to function with multiple vortices if, for example, the curl locations used to begin the analysis were grouped by nearest neighbours to prevent searching between two different vortices.

Using the coordinate transformed data, it is possible to average the tangential velocity around each circumference and identify that the data in Fig. 9 yield a vortex radius (taken as the circumference of maximum average tangential velocity) of approximately 130 m from the identified centre. By normalizing the distance from the centre identified by the proposed method to the other point-identifying methods, it is possible to compare the accuracy of each. Levy et al. (1990), Jeong and Hussain (1995), and Jiang et al. (2002) all identify vortex structures in a region, so they cannot be compared in this manner. However, it is clear that the latter two of these three methods manage to successfully capture the vortex centre point. The Levy et al. (1990) method, however, struggled to provide any region of interest with the given data. Sujudi and Haimes (1995) identify a point as near as 5 m from the centre found with the proposed method but as far away as 2 km, which, when normalized, represents 3.73% and 1630% of the radius of the core, respectively. Finally, Wong and Yip (2009) identify a single point 45 m from the centre (or 34.6% when normalized) even after modifying the methodology to suit the dataset better.

4 Conclusions and Recommendations

A method of identifying the precise location of a tornado's main vortex centre has been developed that allows for superior tracking in comparison to previous work in tornado research, which make assumptions such as the centre being a fixed location, place the vortex a priori, or require user intervention before confirming the centre location. The presented centre-searching method quickly finds solely one centre location for each timestep and horizontal slice of the domain. Previous vortex identification methods have been demonstrated to be deficient in comparison to the presently described method, as they are only able to highlight the region of the vortex, find several centre positions that then require post-processing, or offer an approximate centre location. The benefit of the proposed method is that, having precisely identified the centre of the tornado, one may complete additional analyses on their data to examine the velocity profiles within the vortex, simulate the damage potential relative to the distance from the tornado centre, and track a tornado path throughout its life cycle for both real and simulated vortices. In future work, the scope of the centre searching algorithm may be enhanced by implementing the ability to identify smaller vortices, that may encroach on the main one, or even identify a centre in cases where there are multiple significant vortices that are not clearly stronger than one other.

Acknowledgements The authors should like to thank the Natural Sciences and Engineering Research Council (NSERC) of Canada and the University of Western Ontario for their financial support.

Appendix 1: Summary of Processing Algorithm

The centre of a vortex may be tracked with the proposed method by performing the following series of calculations on a two-dimensional, horizontal slice of data from a tornado dataset. Here, each layer is analyzed without consideration of the layers above or below (Fig. 6a). If not already available in the dataset, the vorticity, $\boldsymbol{\omega}$, is computed for the two-dimensional plane:

$$\boldsymbol{\omega} = \nabla \times \mathbf{u} = \left(\frac{\partial u_z}{\partial y} - \frac{\partial u_y}{\partial z}\right)\widehat{\mathbf{i}} + \left(\frac{\partial u_x}{\partial z} - \frac{\partial u_z}{\partial x}\right)\widehat{\mathbf{j}} + \left(\frac{\partial u_y}{\partial x} - \frac{\partial u_x}{\partial y}\right)\widehat{\mathbf{k}},$$

where $\mathbf{u} = u_x\widehat{\mathbf{i}} + u_y\widehat{\mathbf{j}} + u_z\widehat{\mathbf{k}}$ is the wind-field velocity vector where u_x, u_y, and u_z are the wind speeds in the x-, y-, and z-directions, respectively, but only the $\widehat{\mathbf{k}}$ remains. Then, to ensure that the analysis does not proceed with too many datapoints for each step, a scale is determined based on the resolution and dimensions of the dataset using

$$n = \frac{\min\lfloor n_x,\, n_y \rceil}{c},$$

where n is the scaling-factor (rounded to the nearest integer) based on the size of the dataset, n_x is the number of points in x, n_y is the number of points in y, and c is the scaling parameter (see Appendix 2).

The first n largest curl points (Fig. 6b), $[x_c,\ y_c]$, are spatially averaged using

$$\langle x_c \rangle = \frac{\sum_{i=1}^{n} x_{c,i}}{n},$$

and

$$\langle y_c \rangle = \frac{\sum_{i=1}^{n} y_{c,i}}{n}.$$

The standard deviation, σ, of these locations, in x and y, respectively, is calculated using

$$\sigma_x = \lceil \sqrt{\frac{\sum_{i=1}^{n} \left(x_{c,i} - \langle x_c \rangle\right)^2}{n-1}} \rceil,$$

and

$$\sigma_y = \lceil \sqrt{\frac{\sum_{i=1}^{n} \left(y_{c,i} - \langle y_c \rangle\right)^2}{n-1}} \rceil.$$

The values are rounded up to accommodate that the data locations are not continuous and also to take a more conservative selection approach.

Then, a desired number of standard deviations, s, from the averaged position is selected such that all of the maximum curl locations outside of the bounds of the ellipse, drawn by the following curve, are excluded:

$$\frac{\left(x_{c,i} - \langle x_c \rangle\right)^2}{\left(\sigma_x\right)^2} + \frac{\left(y_{c,i} - \langle y_c \rangle\right)^2}{\left(\sigma_y\right)^2} \leq s.$$

The remaining number of positions, N, will be used as the starting point of lines drawn perpendicular to the vector direction of the datapoint at each location (Fig. 6c). The location of each intersection, $[x_t,\ y_t]$, between each line is computed using

$$x_t = \frac{b_j - b_i}{m_i - m_j},$$

and

$$y_t = \frac{m_j b_i - m_i b_j}{m_j - m_i},$$

where b is the y-intercept of the lines with the domain ordinate, m is the slope of the lines, and i and j are referring to the indexing of each line being compared such that i varies from 1 to $N - 1$ and j from $i + 1$ to N (Fig. 6d). The definition of N is modified to encompass only the intersections that are located within the domain range. The location of $[\langle x_t\rangle,\ \langle y_t\rangle]$ is then computed using

$$\langle x_t\rangle = \frac{\sum_{i=1}^{N} x_{t,i}}{N},$$

and

$$\langle y_t\rangle = \frac{\sum_{i=1}^{N} y_{t,i}}{N}.$$

The standard deviation, σ, of these locations, in x and y, respectively, is calculated using

$$\sigma_{xt} = \lceil\sqrt{\frac{\sum_{i=1}^{N}\left(x_{t,i} - \langle x_t\rangle\right)^2}{N-1}}\rceil,$$

and

$$\sigma_{yt} = \lceil\sqrt{\frac{\sum_{i=1}^{N}\left(y_{t,i} - \langle y_t\rangle\right)^2}{N-1}}\rceil.$$

Then, a desired number of standard deviations, s (its value may differ from that previously used), from the averaged position is selected such that all of the intersections outside of the bounds of the ellipse, drawn by the following curve, are excluded:

$$\frac{\left(x_{t,i} - \langle x_c\rangle\right)^2}{\left(\sigma_{xt}\right)^2} + \frac{\left(y_{t,i} - \langle y_t\rangle\right)^2}{\left(\sigma_{yt}\right)^2} \leq s.$$

From the remaining number of intersections, I, an average location is computed using

$$\langle x_I\rangle = \frac{\sum_{i=1}^{I} x_{t,i}}{I},$$

and

$$\langle y_I\rangle = \frac{\sum_{i=1}^{I} y_{t,i}}{I}.$$

This final location (Fig. 6e) should be a valid position and also sufficiently far from the domain edge such that the subsequent centre search does not attempt to collect data from outside of the domain. In the event that this does occur, the maximum z-vorticity or minimum pressure location can be substituted in place of $[\langle x_I\rangle,\ \langle y_I\rangle]$.

The nearest indexed position to $[\langle x_1 \rangle, \langle y_1 \rangle]$ is used as the centre of a grid of size c-by-c that will be used to identify the tornado centre, defined where there is zero horizontal, storm-relative velocity. The location of minimum velocity of these points is identified and, unless it is actually the tornado centre, is then used as the centre of a new smaller grid of size three-by-three. Each possible combination of loop pattern is identified so that there can be four quadrants made up of four positions in the new grid, four quadrants of six positions in the new grid, and a large loop around the outside of the new grid (see Fig. 7). The values of the signs of the vectors, S, in each loop are summated so that only the loops where this sum is equal to zero are noted as being the possible location of the tornado centre:

$$\sum_{i=1}^{n} S_i = 0.$$

The sum of the magnitude of the tangential velocity vector, u_t, around each of these identified loops is calculated so that the one with the minimum $|u_t|$ sum is taken to be the one with the tornado centre (Fig. 6f):

$$\min \sum_{i=1}^{n} |u_t|_i.$$

If the smaller grid is still too large, the above steps are applied iteratively until the grid is sufficiently small. If there is no path successfully identified, then the above steps are repeated, but the previously identified minimum velocity vector is skipped. The number of repetitions should be limited to a total of c. Should this still fail to yield a path, the point used for the final averaged intersection location may be substituted as the tornado centre.

The four corners of the loop found above are bilinearly interpolated for the position where $u_x = 0$ and $u_y = 0$ (see Fig. 10 a), unless no path is found in which case this interpolation step is omitted. These corner points are arranged such that $x(1) = x(3)$, $x(2) = x(4)$, $y(1) = y(2)$, and $y(3) = y(4)$ and such that $x(1) < x(2)$ and $y(1) > y(3)$ (Fig. 10b). The process of the bilinear interpolation is given for the first step in finding the interpolation of the x-position between points 1 and 2 by

$$x_{12} = x(1) + \left[\frac{0 - u_{y,1}}{u_{y,2} - u_{y,1}}\right](x(2) - x(1)),$$

and 3 and 4 by

$$x_{34} = x(3) + \left[\frac{0 - u_{y,3}}{u_{y,4} - u_{y,3}}\right](x(4) - x(3)),$$

for zero velocity in the y-direction, and then the interpolation of the y-position between points 1 and 3 by

$$y_{13} = y(1) + \left[\frac{0 - u_{x,1}}{u_{x,3} - u_{x,1}}\right](y(3) - y(1)),$$

and 2 and 4 by

$$y_{24} = y(2) + \left[\frac{0 - u_{x,2}}{u_{x,4} - u_{x,2}}\right](y(4) - y(2)),$$

for zero velocity in the x-direction (Fig. 10c). Next, the velocities of these interpolated points are calculated for use in the final interpolation of the position of zero tangential velocity that

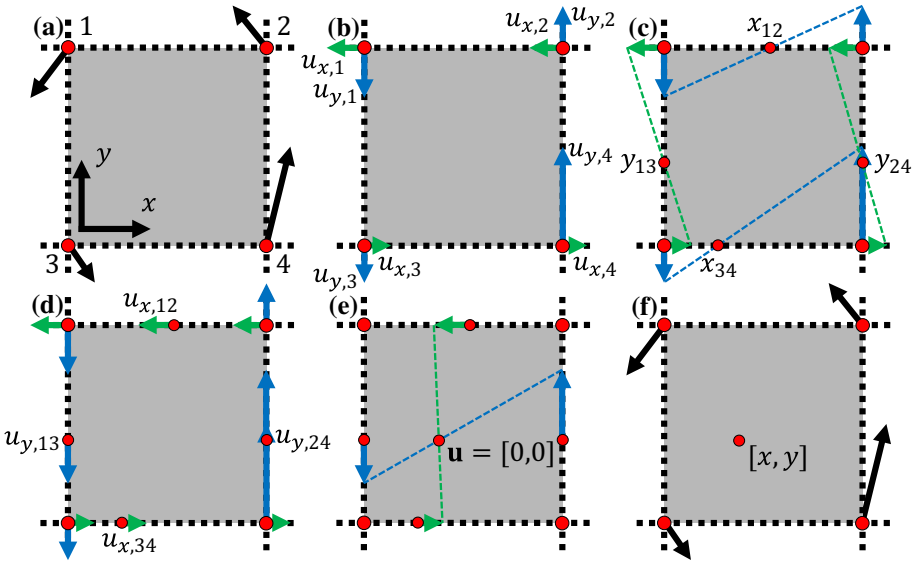

Fig. 10 Finding the tornado centre using artificial data for illustrative purposes as an example. **a** Schematic example of tornado dataset with vectors (shown as black arrows) on an isotropic grid (shown as dashed lines), **b** vector components (x in green and y in blue), **c** location of zero velocity (between x components in green and y components in blue), **d** interpolated vector components, **e** location of zero horizontal velocity (shown as red circle), and **f** tornado centre location

identifies the centre of the tornado. The velocity in the x-direction between points 1 and 2 is interpolated using

$$u_{x,12} = u_{x,1} + \left[\frac{x_{12} - x(1)}{x(2) - x(1)}\right]\left(u_{x,2} - u_{x,1}\right),$$

then in the x-direction between points 3 and 4 using

$$u_{x,34} = u_{x,3} + \left[\frac{x_{34} - x(3)}{x(4) - x(3)}\right]\left(u_{x,4} - u_{x,3}\right),$$

in the y-direction between points 1 and 3 using

$$u_{y,13} = u_{y,1} + \left[\frac{y_{13} - y(1)}{y(2) - y(1)}\right]\left(u_{y,3} - u_{y,1}\right),$$

and finally, in the y-direction between points 2 and 4 using (Fig. 10d)

$$u_{y,24} = u_{y,2} + \left[\frac{y_{24} - y(2)}{y(4) - y(2)}\right]\left(u_{y,4} - u_{y,2}\right).$$

Hence, the x and y positions of zero tangential velocity between these calculated velocities can be interpolated to identify the centre of the tornado (Fig. 10e)

$$x = x_{12} + \left[\frac{0 - u_{x,12}}{u_{x,34} - u_{x,12}}\right](x_{34} - x_{12}),$$

and

$$y = y_{13} + \left[\frac{0 - u_{y,13}}{u_{y,24} - u_{y,13}}\right](y_{24} - y_{13}),$$

which concludes the searching portion of the algorithm (Fig. 10f).

Appendix 2: Comparison of Scale Factor, *c*

To test the effects of changing the number of points selected in the maximum curl identification process, c was varied from 1 to 10, as an integer only for simplicity, and, based on trial-and-error, was found to be an appropriate range. Although the overall effect of changing this value appears to be minimal, selecting an extreme value in this range will quickly deteriorate the accuracy of the centre detection capabilities of the proposed method and increase the chance of another smaller, less-defined vortex being included in the search (see Table 3).

An optimum value of $c = 6$ was determined for the current data based on the least number of errors and re-attempts, even though a non-integer value may be optimal. The paths determined for each different c-value can be seen in Fig. 11. Adjusting c appears to only affect the searching algorithm negatively at either end of the range selected. This is because it begins to either exclude so many points that almost none are left for the analysis or, at the other extreme, include so many points that the selection criterion of maximum curl becomes meaningless. This scaling factor acts as a tool to eliminate the many data points identified as having a high curl but that only represent partially formed or small vortices and would otherwise skew the centre locating of the program. It should only need to be adjusted once by the user for a given dataset before proceeding with further analyses.

The searches performed neglected the results of the search from each preceding timestep, resulting in errors introduced by sweeping through the entire domain unnecessarily. Given the high spatial and temporal resolution of the dataset used in this paper, the search domain after the centre is successfully located the first time may be reduced to a very small region and carried through to each subsequent timestep processed.

Table 3 Comparison of the number of times the programme failed to find a loop about a centre and/or interpolate for a centre using different c values

c Value	Number of re-attempts	Number of failed attempts	Failure rate (%)
1	19	268	20.60
2	11	65	5.00
3	5	14	1.00
4	5	1	0.08
5	5	1	0.08
6	3	1	0.08
7	4	1	0.08
8	4	1	0.08
9	5	3	0.23
10	6	4	0.31

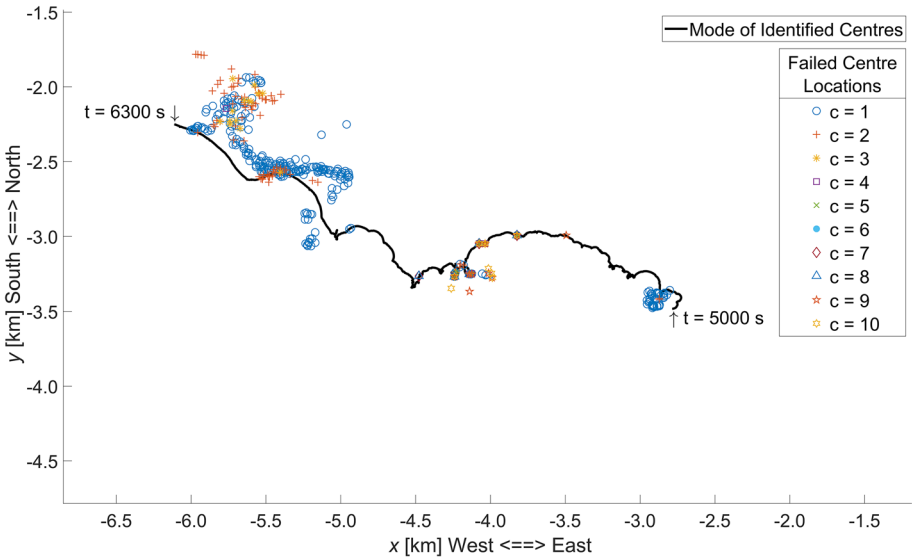

Fig. 11 Comparing the mode of identified tornado centre points, found by varying c, with the failed results of the different c values used. The data shown are taken relative to the simulation domain for all timesteps at height $z = 15$ m a.g.l

References

Aboelkassem Y, Vatistas GH, Esmail N (2005) Viscous dissipation of Rankine vortex profile in zero meridional flow. Acta Mech Sinica 21(6):550–556

Agee E, Taylor L (2019) Historical analysis of US tornado fatalities (1808–2017): population, science, and technology. Weather Clim Soc 11(2):355–368

Altalmas A, El Damatty AA (2014) Finite element modelling of self-supported transmission lines under tornado loading. Wind Str 18(5):473–495

Baker CJ, Sterling M (2017) Modelling wind fields and debris flight in tornadoes. J Wind Eng Ind Aerodyn 168:312–321

Beck V, Dotzek N (2010) Reconstruction of near-surface tornado wind fields from forest damage. J Appl Meteorol Climatol 49(7):1517–1537

Brooks HE, Correia J (2018) Long-term performance metrics for national weather service tornado warnings. Weather Forecast 33(6):1501–1511

Bryan G (2008) CM1 Homepage. In: University Corporation for Atmospheric Research. http://www2.mmm.ucar.edu/people/bryan/cm1/. Accessed 29 June 2020

Bryan GH, Fritsch JM (2002) A benchmark simulation for moist nonhydrostatic numerical models. Mon Weather Rev 130(12):2917–2928

Chen Q, Zhong Q, Qi M, Wang X (2015) Comparison of vortex identification criteria for planar velocity fields. Phys Fluids 27(8):085101

Church CR, Snow JT, Baker GL, Agee EM (1979) Characteristics of tornado-like vortices as a function of swirl ratio: a laboratory investigation. J Am Meteorol Soc 36(9):1755–1776

Curtis A, Mills JW (2012) Spatial video data collection in a post-disaster landscape: the Tuscaloosa tornado of April 27th 2011. Appl Geogr 32(2):393–400

Davies-Jones R (2008) Can a descending rain curtain in a supercell instigate tornadogenesis barotropically? J Atmos Sci 65(8):2469–2497

Doswell CA, Moller AR, Brooks HE (1999) Storm spotting and public awareness since the first tornado forecasts of 1948. Weather Forecast 14(4):544–557

Finley CA, Orf L, Lee BD, Wilhelmson RB (2018) High-resolution simulation of a violent tornado in the 27 April 2011 outbreak environment. In: Proceedings of the 29th Conference on Severe Local Storms,

Pinnacle AB. Am Meteorol Soc. https://ams.confex.com/ams/29SLS/webprogram/Paper348812.html. Accessed 1 Sep 2020
Grams JS, Thompson RL, Snively DV, Prentice JA, Hodges GM, Reames LJ (2012) A climatology and comparison of parameters for significant tornado events in the United States. Weather Forecast 27:106–123
Hamada A, El Damatty AA (2011) Behaviour of guyed transmission line structures under tornado wind loading. Comput Str 89(11–12):986–1003
Jeong J, Hussain F (1995) On the identification of a vortex. J Fluid Mech 285:69–94
Jiang M, Machiraju R, Thompson D (2002) A novel approach to vortex core region detection. In: Elbert D, Brunet P, Navazo I (eds) Joint Eurographics-IEEE TCVG symposium on visualization, vol. 2, pp 217–225
Jiang M, Machiraju R, Thompson D (2005) Detection and visualization of vortices. In: Hansen CD, Johnson CR (eds) The visualization handbook. Elsevier Academic Press, Oxford, pp 295–309
Karstens CD, Gallus WA, Lee BD, Finley CA (2013) Analysis of tornado-induced tree fall using aerial photography from the Joplin, Missouri, and Tuscaloosa-Birmingham, Alabama, tornadoes of 2011. J Appl Meteorol Climatol 52(5):1049–1068
Kuo HL (1971) Axisymmetric flows in the boundary layer of a maintained vortex. J Atmos Sci 28:20–41
Levy Y, Degani D, Seginer A (1990) Graphical visualization of vortical flows by means of helicity. AIAA J 28(8):1347–1352
Lewellen WS (1993) Tornado vortex theory. In: Church C, Burgess D, Doswell C, Davies-Jones R (eds) The tornado: its structure, dynamics, predictions, and hazards. Am Geophys Union, Washington, 79:19–39
Lim JR, Liu BF, Egnoto M (2019) Cry wolf effect? Evaluating the impact of false alarms on public responses to tornado alerts in the southeastern United States. Weather, Clim, Soc 11(3):549–563
Liu Z, Zhang C, Ishihara T (2018) Numerical study of the wind loads on a cooling tower by a stationary tornado-like vortex through LES. J Fluids Str 81:656–672
Natarajan D (2011) Numerical simulation of tornado-like vortices. PhD dissertation, The University of Western Ontario, Ontario, Canada
National Centers for Environmental Information [NCEI] (2021a) Billion-dollar weather and climate disasters. Natl Oceanic Atmos Adm. https://www.ncdc.noaa.gov/stormevents/. Accessed 2 February 2022.
National Centers for Environmental Information [NCEI] (2021b) Storm events database. Natl Oceanic Atmos Adm. https://www.ncdc.noaa.gov/billions/events/US/1980-2021b. Accessed 2 February 2022.
Orf L (2019) A violently tornadic supercell thunderstorm simulation spanning a quarter-trillion grid volumes: computational challenges, I/O framework, and visualizations of tornadogenesis. Atmos 10(10):578–601
Orf LG, Semeraro BD, Wilhelmson RB (2007) Vortex detection in a simulated supercell thunderstorm. Atmos Sci Lett 8:29–35
Orf L, Wilhelmson R, Wicker L (2016) Visualization of a simulated long-track EF5 tornado embedded within a supercell thunderstorm. Parallel Comput 55:28–34
Pecin TG, Almeida AAD, Roehl JL (2011) Tornadic mechanical global actions on transmission towers. J Brazilian Soc of Mech Sci Eng 33(2):131–138
Potvin CK (2013) A variational method for detecting and characterizing convective vortices in Cartesian wind fields. Mon Weather Rev 141(9):3102–3115
Rankine WJM (1877) Motions of fluids – hydrodynamics. Manual of Appl Mech. Charles Griffin and Company, London, pp 574–577
Razavi A, Sarkar PP (2018) Laboratory study of topographic effects on the near-surface tornado flow field. Boundary-Layer Meteorol 168(2):189–212
Refan M (2014) Physical simulation of tornado-like vortices. PhD dissertation, The University of Western Ontario, Ontario, Canada
Refan M, Hangan H (2016) Characterization of tornado-like flow fields in a new model scale wind testing chamber. J Wind Eng Ind Aerodyn 151:107–121
Refan M, Hangan H, Wurman J, Kosiba K (2017) Doppler radar-derived wind field of five tornado events with application to engineering simulations. Eng Str 148:509–521
Rosen KH (2000) Handbook of discrete and combinatorial mathematics. CRC Press, Boca Raton
Savory E, Parke GAR, Zeinoddini M, Toy N, Disney P (2001) Modelling of tornado and microburst-induced wind loading and failure of a lattice transmission tower. Eng Str 23(4):365–375
Shehata AY, El Damatty AA, Savory E (2005) Finite element modeling of transmission line under downburst wind loading. Finite Elem Anal Des 42:71–89
Strawn RC, Kenwright DN, Ahmad J (1999) Computer visualization of vortex wake systems. AIAA J 37(4):511–512
Sujudi D, Haimes R (1995) Identification of swirling flow in 3-D vector fields. In: Proceedings of the 12th computational fluid dynamics conference, fluid dynamics and co-located conferences, San Diego, USA A95–36567

Tang Z, Feng C, Wu L, Zuo D, James DL (2018) Characteristics of tornado-like vortices simulated in a large-scale ward-type simulator. Boundary-Layer Meteorol 166(2):327–350
Ward NB (1972) The exploration of certain features of tornado dynamics using a laboratory model. J Atmos Sci 29(6):1194–1204
Wan CA, Chang CC (1972) Measurement of the velocity field in a simulated tornado-like vortex using a three-dimensional velocity probe. J Atmos Sci 29:116–127
Wang J, Cao S, Pang W, Cao J (2017) Experimental study on effects of ground roughness on flow characteristics of tornado-like vortices. Boundary-Layer Meteorol 162(2):319–339
Wen Y-K (1975) Dynamic tornadic wind loads on tall buildings. J Str Div 101:169–185
Wen Y-K, Ang AH-S (1975) Tornado risk and wind effects on structures. In: Eaton KJ (eds) Proceedings of the 4th international conference on wind effects on buildings and structures, London, UK, pp 63–74
Wong KY, Yip CL (2009) Identifying centers of circulating and spiraling vector field patterns and its applications. Ptrn Recognit 42(7):1371–1387
Wood VT, Brown RA (1992) Effects of radar proximity on single-Doppler velocity signatures of axisymmetric rotation and divergence. Mon Weather Rev 120(12):2798–2807